Journal of Nuclear Materials 407 (2010) 171–177

Contents lists available at ScienceDirect

Journal of Nuclear Materials

journal homepage: www.elsevier.com/locate/jnucmat

Effects of dissolved oxygen on electrochemical and semiconductor properties of 316L stainless steel

Zhicao Feng, Xuequn Cheng *, Chaofang Dong, Lin Xu, Xiaogang Li *

Corrosion and Protection Center, University of Science and Technology Beijing, Beijing 100083, China

ARTICLE INFO

Article history:
Received 8 April 2010
Accepted 13 October 2010

ABSTRACT

The effects of dissolved oxygen on the electrochemical behavior and semiconductor properties of passive film formed on 316L SS in three solutions with different dissolved oxygen were studied by using polarization curve, Mott–Schottky analysis and the point defect model (PDM). The results show that higher dissolved oxygen accelerates both anodic and cathodic process. Based on Mott–Schottky analysis and PDM, the key parameters for passive film, donor density N_d, flat-band potential E_{fb} and diffusivity of defects D_0 were calculated. The results display that N_d($1-7\times10^{27}$ m^{-3}) and D_0($1-18\times10^{-16}$ cm^2/s) increase and E_{fb} value reduces with the dissolved oxygen in solution.

1. Introduction

Stainless steels are usually used in environments that contain oxygen, so it is useful to consider how dissolved oxygen in solution affects the electrochemical behavior of passive film formed on stainless steel. Over last several decades, there have been numerous efforts in such field. Obviously, the oxygen reduction reaction is one of the most relevant cathodic processes in different fields of the electrochemistry. Qiao et al. [1] has tried to make an apparent relationship between effects of oxygen and corrosion process of high nitrogen bearing stainless steel. It is indicated that saturating 0.05 M H_2SO_4 solution with nitrogen to remove oxygen from the system decreased the potential slightly in negative direction and reduced the current densities below that of the aerated solution.

Moreover, many other authors have researched the influences of dissolved oxygen on the structure, composition and growth of passive films formed on metal or alloy. A study [2] about oxygen evolution and porous anodic alumina formation believed that the reaction of oxygen evolution during anodization plays a crucial role in determining the morphology of anodic films. It believed that the oxygen bubbles evolved during anodization under normal atmospheric pressure cannot leave from the film surface immediately due to the adsorption of the film surface, which caused many pores and grooves in the alumina layer. Another deeper study [3] about residual flaws due to formation of oxygen bubbles in anodic alumina suggested that the formation of oxygen bubbles within anodic alumina, by oxidation of O^{2-} ions in the vicinity of the metal/film interface, are considered as one type of residual flaw, which are the preferred sites of pitting and dielectric breakdown. So, enough oxygen bubbles in the solution are able to change the structure, morphology and growth of passive films, which directly affect the anodic dissolution of metal.

Besides of the effects of oxygen on electrochemical behavior, that on the semiconductor properties of passive films also needs our more attentions. In general, the passive films of metal are mainly made up of metallic oxides or hydroxides which are envisaged as semiconductors. Mott–Schottky analysis, as a good method, has been widely used to study and characterize the semiconductor properties of passive films, such as the passive films on chromium, nickel, aluminum and stainless steels [4–7]. Fattah-alhosseini et al. [8] used Mott–Schottky analysis and point defect model (PDM) to investigate the effects of H_2SO_4 solution concentration on semiconductor properties of passive films formed on stainless steels. They indicated that the diffusivities and densities of the defects within the passive film increased with the H_2SO_4 solution concentration. And the passive films formed on stainless steels at different potentials in acids solution all performed n-type semiconductor property.

Although the relationship between dissolved oxygen and electrochemical behavior of passive film formed on stainless steels is made clear by previous authors, unfortunately a complete understanding of how oxygen influenced stainless steel passive layer is still lacking. This, however, is a key point for the comprehension of many corrosion mechanisms. In this paper, according to a variety of techniques, including potentiodynamic polarization, Mott–Schottky analysis and PDM, we give a full explanation to the effects of dissolved oxygen in the borate buffer solution on cathodic and anodic process of 316L SS. And three parameters, donor density N_d, flat-band potential E_{fb} and diffusion coefficient D_0, are calculated in this paper, which could accurately characterize the corrosion resistance of passive film. More importantly, the

* Corresponding authors. Tel.: +86 10 62333931; fax: +86 10 62334005.
E-mail addresses: chxq2000@hotmail.com (X. Cheng), lixiaogang99@263.net (X. Li).

0022-3115/$ - see front matter © 2010 Elsevier B.V. All rights reserved.
doi:10.1016/j.jnucmat.2010.10.010

relationship between dissolved oxygen and such parameters is given in this paper. It is quite useful to understand the effects of oxygen on properties of passive film.

2. Experimental

2.1. Electrodes and solutions

The 316L stainless steel was investigated in this paper, with the chemical composition (in wt.%): 0.60Si, 0.80Mn, 0.013P, 2.28Mo, 17.14Cr, 12.58Ni, 0.014C, 0.073S. The specimen with the size of 10 mm × 10 mm × 3 mm was soldered to a copper wire for electrical connection, using lead-containing solder and phosphoric acid flux, and was mounted in epoxy resin with only 1 cm^2 of surface area exposure to solution. The working surface of the specimen was abraded to a mirror finish with 2000 SiC paper, cleaned with distilled water and acetone, and then dried in cold air immediately before electrochemical tests. Electrochemical experiments were carried out on a Vmp3 advanced electrochemical system from Princeton Applied Research. A saturated calomel electrode (SCE) and a large graphite plate served as the reference electrode and the counter electrode respectively. All experiments in this paper were conducted in borate buffer solution 0.05 M H_3BO_3 + 0.075 M $Na_2B_4O_7{\cdot}10H_2O$ (pH 9.0) at 22 °C, in which different dissolved oxygen contents were controlled by blowing N_2, O_2 and no blowing gas respectively.

2.2. Open-circuit potential measurement in situ

The working specimen was polarized potentiostatically in electrolyte for 10 min at −1.3 V_{SCE} to remove the air-formed film before all electrochemical experiments. The open-circuit potential (OCP) of the specimen was performed in static electrolyte (without blowing gas). Until the OCP values were stable enough, O_2 gas was blown smoothly into the solution with the gas-guide tube close to the inner side of the electrolytic cell. During the process of saturating the solution with oxygen, the OCP measurement was still running.

2.3. Potentiodynamic polarization and EIS measurements

The potentiodynamic polarization tests in solutions with different dissolved oxygen were carried out on the potential scan rate of 1 mV/s and the potential range from −0.8 V_{SCE} to 1.1 V_{SCE} for evaluating the electrochemical corrosion behavior. Before the electrochemical impedance spectroscopy (EIS), the specimens firstly were polarized at −0.2 V_{SCE}, −0.1 V_{SCE}, 0 V_{SCE}, 0.1 V_{SCE}, and 0.2 V_{SCE} respectively for 2 h to ensure that stable enough film was formed on the specimen. The EIS experiment was conducted over the frequency from 100 kHz to 2 mHz using a 10 mV sinusoidal potential modulation (peak to peak) around the film formation potentials.

2.4. Mott–Schottky measurements

Mott–Schottky analysis was employed to characterize the semiconducting properties of the passive film formed in solutions with different dissolved oxygen, before which the specimen was polarized at −0.2 V_{SCE}, −0.1 V_{SCE}, 0 V_{SCE}, 0.1 V_{SCE}, and 0.2 V_{SCE} respectively for 2 h. Potential sweeps are carried out from −0.3 V_{SCE} to 0.6 V_{SCE} with an amplitude signal of 10 mV, at a scan rate of 20 mV/s. In view of the controversy about the measured frequency between the literatures indicating that the electronic properties of the passive layer do not change with the frequency at 600–6000 Hz, and others holding that the capacitance vary a lot with the frequency [9,10], The very commonplace frequency value 1000 Hz was used in this investigation.

3. Results and discussion

3.1. Open-circuit potential measurement in situ

In Fig. 1, OCP plots of the specimen recorded in 0.05 M H_3BO_3 + 0.075 M $Na_2B_4O_7{\cdot}10H_2O$ solution are reported before and after blowing oxygen. It is obvious that before saturating the solution with oxygen, the OCP values of specimen are stable enough around −0.25 V_{SCE} at 1800 s. And then oxygen is blown smoothly into solution with the gas-guide tube close to the inner side of the vessel. During the process of blowing air, the solution stirring caused by the air bubble moving upward to fluid level is ignored because of blowing slowly enough and the far distance between the gas-guide tube and working electrode. After blowing oxygen for half an hour, it can be seen from Fig. 1 that the OCP values decrease sharply from −0.25 V_{SCE} to another stable enough potential value around −0.38 V_{SCE}. And then, oxygen is stopped to be blew into solution, the OCP values of the working electrode are not variable in solution. Around 7000 s, oxygen is started to be blew into solution again, however the OCP values of specimen still do not change, which suggests that the dissolved oxygen is saturated enough that the redundant oxygen blowing has little influence on the OCP values.

The value of OCP is defined as the potential drop in Helmholtz double layers, which strongly depends on the surface state of passive films formed on specimens. This means that negative and positive charges respectively occupying both sides of Helmholtz double layers are equilibrium at 1800 s, so OCP reach the stable value at 1800 s. After 1800 s, oxygen is started to be blew into solution. The introduction of oxygen changes the surface state of passive film, further disturbs the equilibrium distribution of charges in Helmholtz double layers, and finally makes them to another equilibrium state at which the potential drop in Helmholtz double layers is more negative. It is because higher oxygen in solution most likely results in more oxygen vacancies in the surface of passive film, which would be demonstrated in later evidences. Such vacancies serve as a kind of trap accumulating negative charges in the surface of passive film, which causes the more negative potential drop in Helmholtz double layers. So, the stable OCP values of 316L stainless steels decrease with the dissolved oxygen.

3.2. Potentiodynamic polarization

Fig. 2 displays the polarization curves for the 316L SS in borate buffer solution with different dissolved oxygen contents. From Fig. 2, we can clearly figure out the following results: (1) E_{corr2},

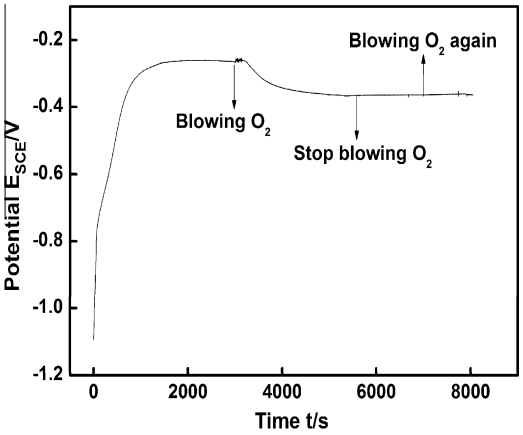

Fig. 1. Evolution with time of the open-circuit potential of 316L SS in borate buffer solution before and after blowing O_2.

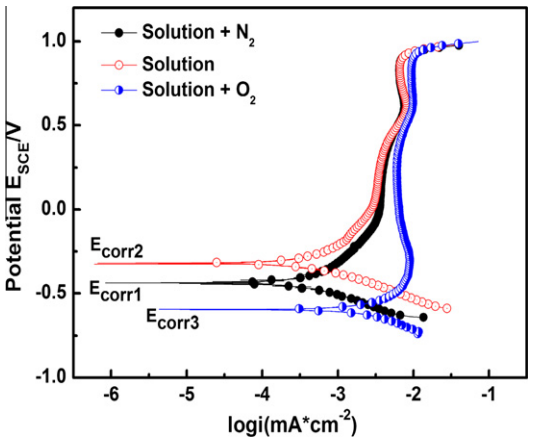

Fig. 2. Potentiodynamic polarization curve for 316L SS in borate buffer solution with different dissolved oxygen. The scan rate was 1 mV/s.

the value of corrosion potential in solution, is larger than that in solution with saturated nitrogen, E_{corr1}. This means that saturating the solution with nitrogen to eliminate oxygen from the solution is found to decrease the potential slightly in the negative direction. (2) Meanwhile, blowing nitrogen into solution also brings down the cathodic current density, which indicates that the decrease of dissolved oxygen apparently influences on the cathodic process. However it has few influences on anodic process, since two anodic curves are almost overlapping. (3) E_{corr3}, the corrosion potential in solution with saturated oxygen, is much lower than E_{corr1} and E_{corr2}. Moreover, the passive current I_p of the specimen in saturated oxygen solution is largest. So, blowing oxygen into solution directly influences the anodic process. In sum, the low content of dissolved oxygen in solution increases the corrosion potential E_{corr} and only affects cathodic process; while the high dissolved oxygen reduces the value of E_{corr} and influences both anodic and cathodic process.

Based on the experimental results in Fig. 2, dissolved oxygen content in solution remarkably affects the corrosion behavior of the 316L SS. The ideal polarization curves in Fig. 3 are used to explain the effects of oxygen concentration. The curve A_1 represents the possible ideal anodic polarization curve of 316L SS in solution;

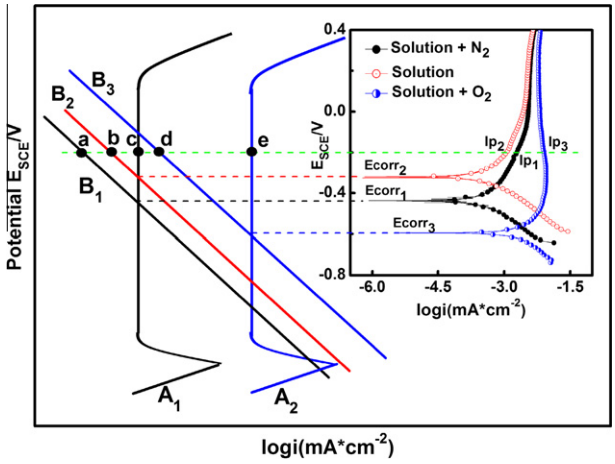

Fig. 3. Supposed diagram of ideal polarization curves for the borate buffer solution with different dissolved oxygen. A_1 and B_1 represent the anodic polarization curve and the cathodic curve respectively in solution with saturated nitrogen; A_1 and B_2 for the curves in solution; A_2 and B_3 for the curves in solution with saturated oxygen.

while the curve B_2 represents the ideal cathodic reaction of O_2 reduction. It is easy to find out that there is a point of intersection between anodic curve A_1 and cathodic curve B_2, which represents the corrosion potential E_{corr2}. The cathodic reaction is:

$$4OH^- \Longleftrightarrow O_2 + 2H_2O + 4e \quad (1)$$

$$E_{OH^-/O_2} = E^{\Theta}_{OH^-/O_2} + \frac{RT}{4F}\ln\frac{p_{O_2}}{a^4_{OH^-}} \quad (2)$$

where E_{OH^-/O_2} is the equilibrium potential of Eq. (1); $E^{\Theta}_{OH^-/O_2}$ is the standard equilibrium potential of Eq. (1); R is gas constant; T is the absolute temperature; F is the Faraday's constant; Po_2 is the oxygen partial pressure and a_{OH^-} is activity coefficient of OH^-.

From the Eq. (2), E_{OH^-/O_2} is closely related with the partial pressure of oxygen Po_2. The value of E_{OH^-/O_2} decreases as Po_2 reduces. So, when slowly blowing nitrogen into solution to eliminate oxygen, the ideal cathodic polarization curve will move slightly in the negative direction, which explains how dissolved oxygen affects the cathodic process. Until the solution full of saturated nitrogen, the ideal cathodic polarization curve finally becomes into curve B_1. If blowing nitrogen into solution has few influences on the anodic process, the corrosion process in solution with saturated nitrogen will be composed of cathodic curve B_1 and anodic A_1. In this case, the point of intersection of curve A_1 and B_1 represents the corrosion potential E_{corr1}, which explains why the value of E_{corr2} in the solution is higher than E_{corr1} in saturated nitrogen solution.

Likewise, when slowly saturating the solution with oxygen, the ideal cathodic polarization oxygen would move in the positive direction according to the Eq. (2), finally to B_3. Meanwhile, the dissolved oxygen in solution is enough to influence the anodic process, which makes the ideal anodic polarization curve move to A_2. The reason why saturated oxygen results in the anodic curve right shift will be explained in later discussions. So, the corrosion behavior in solution with saturated oxygen is made up of curves A_2 and B_3. The point of intersection of the two curves represents the corrosion potential E_{corr3}, which is lower than E_{corr1} and E_{corr2}. This is a good agreement with the result of OCP measurement in situ that OCP value became more negative when increasing dissolved oxygen in solution. Therefore, the movements of the ideal polarization curves caused by dissolved oxygen give a good explanation to the variability of corrosion potential E_{corr}.

Besides of the discussions above, the movements of polarization curves are also used to explain the change of current densities. In Fig. 3, there are five points of intersection (a, b, c, d, and e) of the line at -0.2 V_{SCE} and ideal polarization curves. Understandably, the segments bc, ac and de express the values of passive current densities I_{p2}, I_{p1} and I_{p3} respectively. It can be easy seen from Fig. 3 that the length of segment bc is the shortest, de is the longest and ac is in the middle. This quite accurately corresponds to the order of passive current densities: $I_{p2} < I_{p1} < I_{p3}$. It demonstrates that it is reasonable to use the movements of ideal polarization curves to explain the effects of dissolved oxygen on the corrosion process.

3.3. Semiconductor properties

Based on the Mott–Schottky theory [11], the relationship between the space charge capacitance C and the applied potential E can be written as:

$$\frac{1}{C^2} = \frac{2}{\varepsilon\varepsilon_0 eNA^2}(E - E_{fb} - KT/e) \quad \text{n-type} \quad (3)$$

$$\frac{1}{C^2} = \frac{-2}{\varepsilon\varepsilon_0 eNA^2}(E - E_{fb} - KT/e) \quad \text{p-type} \quad (4)$$

where E_{fb} is the flat-band potential; ε_0 is the vacuum permittivity with the value of 8.85×10^{-14} F/cm; ε is the relative dielectric constant of the specimen, 15.6 as in the literature [12]; K is the Boltzmann constant (1.38×10^{-23} J/K); T is the absolute temperature; $N(m^{-3})$ is the donor density (N_d) or accept density (Na) and A is the surface area of the sample (cm^2).

In this paper, it is assumed that the measured capacitance corresponds to the space charge capacitance and that extra series capacitance, such as the Helmholtz capacitance and surface state capacitance, can be ignored [13,14]. This assumption is reliable because the Helmholtz capacitance with the value of 30–50 μF/cm^2 for the smooth metallic/solution interface is much higher than the capacitances tested on our specimens.

Fig. 4 displays the Mott–Schottky plots for the passive films formed on 316L SS in borate buffer solution with different dissolved oxygen. Before the measurement, the specimens were pre-passivated for 2 h at −0.2 V_{SCE}, 0 V_{SCE}, 0.1 V_{SCE} and 0.2 V_{SCE} respectively. From Fig. 4b–d, in the potential range from −0.3 V_{SCE} to 0.3 V_{SCE}, a linear relationship can be observed between C^{-2} and E in three solutions, the slopes can be identified. According to the Eq. (3), the positive slopes indicate all the passive films formed on specimens perform n-type semiconductor. The appearance of peak values in Fig. 4 represents an inversion from n-type to p-type semiconductor property. We should notice that in all film formation potentials, the passive films formed in the solution with higher dissolved oxygen possess lower slope values.

Moreover, the donor density (N_d) can be calculated from the slope of Mott–Schottky plots. Fig. 5 displays donor densities of the films formed at different potentials in three solutions. N_d value increases with the dissolved oxygen and reduces with the film formation potential changing to positive direction, which is in accordance with the results obtained in previous studies [8,15]. It is acceptable that the carrier density closely associates with the chance of the corrosion reaction since it corresponds to the point defects and the nonstoichiometry of the space charge region. So, the variability of donor densities indicates the change of structure and morphology in the passive film. Many previous works [16,17] suggested that the smaller N_d would cause the lower possibilities of film breakdown and pitting initiation, because defects in the film are potential sites where corrosion process are more likely to occur. Thus, higher dissolved oxygen in solution which causes the larger donor densities would probably accelerate metal dissolution. It clearly explains effects of dissolved oxygen on anodic polarization curve right shift in Fig. 3.

According to the Eq. (3), the other semiconductor parameter (flat-band potential E_{fb}) is obtained in three solutions, as shown in Table 1. In all film formation potentials, the values of E_{fb} for the passive film become more negative with the increase of dissolved oxygen in solution. Such variability of E_{fb} is ascribed to the change of metal/solution interface in three solutions. The Nernstian expression for the E_{fb} of a semiconductor is:

$$E_{fb} = -E_F^0/q + \Delta\Phi_H \tag{5}$$

$$\Delta\Phi_H = 0.059(pzc - pH) \tag{6}$$

where pzc is the point of zero charge at which the surface excesses of H^+ and OH^- are equal under the condition of no other specifically

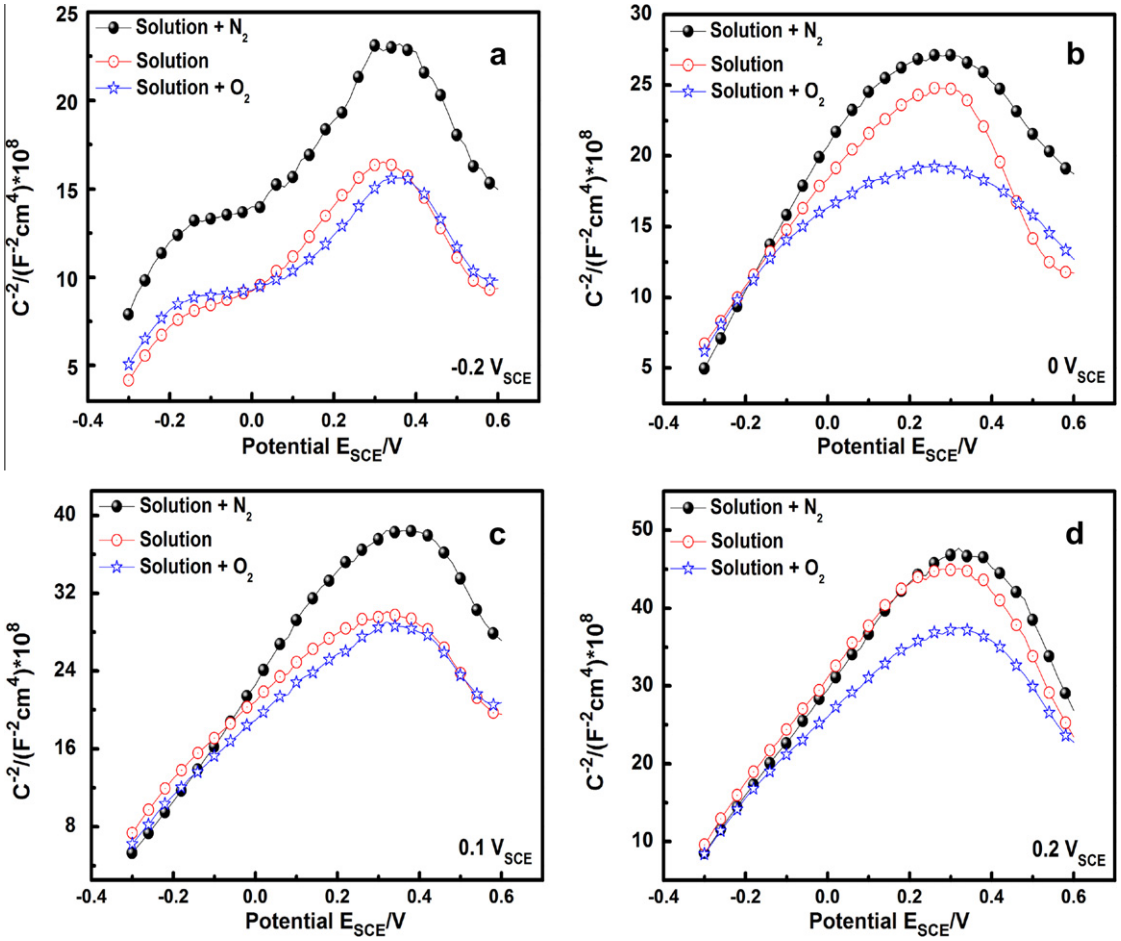

Fig. 4. Mott–Schottky plots measured in borate buffer solution. The electrode is pre-passivated for 2 h at (a) −0.2 V_{SCE}, (b) 0 V_{SCE}, (c) 0.1 V_{SCE} and (d) 0.2 V_{SCE} respectively.

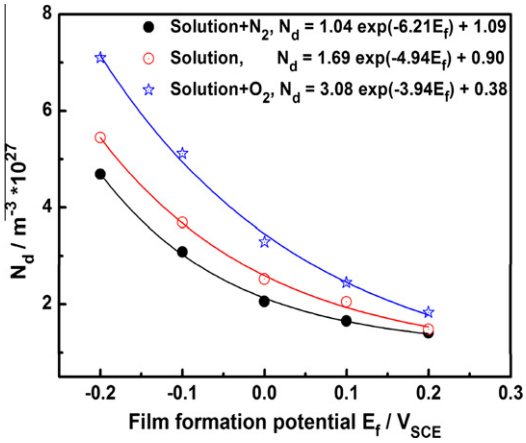

Fig. 5. N_d–E_f curves of the passive film formed on 316L SS in borate buffer solution with different dissolved oxygen.

Table 1
Flat-band potentials of passive film formed on 316L SS at each film formation potential in solution with different dissolved oxygen.

Formation potential E_f /V_{SCE}	Flat-band potential E_{fb}/V		
	Solution + N_2	Solution	Solution + O_2
0	−0.43	−0.51	−0.58
0.1	−0.39	−0.50	−0.51
0.2	−0.43	−0.49	−0.52

adsorbed species except for H^+ and OH^- in solution; E_F^0 is the Fermi level of a semiconductor material at *pzc*; and $\Delta\Phi_H$ is the potential drop in Helmholtz layer. From the Eq. (5), E_{fb} varies with E_F^0 and $\Delta\Phi_H$. It is assumed that the Fermi levels of specimens in three solutions are constant because of the following aspects. One aspect is that only one specimen was tested repeatedly in all solutions, which avoids the attendance of adulterate behavior caused by the differences of specimens (structure, composition, defects in the surface). The other aspect is that dissolved oxygen content have fewer influences on the dominate components in the passive films of specimen. Thus, the variation of E_{fb} is attributed to the change of $\Delta\Phi_H$ in the system. The value of $\Delta\Phi_H$ is defined as the difference between the potential at the electrode surface which is determined by the surface charge (q_s) and the potential at the outer Helmholtz plate (ohp) [11]. Specifically adsorbed anions on the passive film are closely related with $\Delta\Phi_H$. In our research, before blowing O_2 into the solution, the specifically absorbed anions on the passive film are mainly borate anions. After blowing O_2 into the solution, more dissolved oxygen occur reduction reaction, which indicates the specific adsorption of borate anions were partly substituted by O^{2-} or OH^-. Because of the smaller size of O^{2-} and OH^-, more negative charges accumulated on the surface, which causes an increase of residual negative charges in the surface, further makes potential drop in Helmholtz layer more negative. This clearly explains why the flat-band potentials become more negative with the increase of dissolved oxygen in solution. Moreover, the adsorbed anion O^{2-} or OH^- on the passive film is beneficial to the corrosion behavior, since they play a more important role in the reaction of metal dissolution than borate anions do. So, higher dissolved oxygen in solution speeds up the anodic reaction. It further explains the shift of anodic polarization curve in Fig. 3.

3.4. PDM and diffusivity of point defects

3.4.1. Point defect model

The PDM [18,19] claims that the point defects present in a barrier layer generally are cation vacancies ($V_M^{\chi'''}$), oxygen vacancies (V_O'') and cation interstitials ($M_i^{\chi+}$). Cation vacancies are electron acceptors, doping the barrier layer p-type, whereas oxygen vacancies and metal interstitials are electron donors, resulting in n-type doping. The Mott–Schottky analysis indicates the passive films of 316L SS in three solutions perform n-type semiconductor property, so point defects presenting in the passive film mainly are oxygen vacancies (V_O'') and interstitials cation ($M_i^{\chi+}$). In view of the apparent difference of atomic radius between Fe and O, it is obviously figured out that the atomic radius of Fe is much larger than that of O, which means interstitials iron Fe_i^{2+} needs much more energy to move in the passive film. Compared with interstitials cation, it is easier for oxygen vacancies to flux in the passive film, so the major point defects in the passive film are oxygen vacancies. This is a good agreement with the results of Kloppers [20], who insisted oxygen vacancies gave a more important contribution to passive current densities than interstitials iron does and the principal defects in passive film of iron alloy are oxygen vacancies. Thus, in the set of defect generation and annihilation reactions occurring at the metal/barrier interface and at the barrier layer-solution interface in Fig. 6 [8], we are greatly concerned the generation and annihilation reactions of oxygen vacancies in this paper. The Eq. (8) indicates that the number of oxygen vacancies in the barrier layer increases when blowing oxygen into solution. So, the passive films of 316L SS formed in the solution with saturated O_2 contain more defects of oxygen vacancies than that in the solution with N_2. Such defects in the film provide potential sites where anodic dissolutions are more likely to occur. It gives a good interpretation for the effects of dissolved oxygen on the anodic process, and also explains the positive shift of ideal anodic polarization curve in Fig. 3.

3.4.2. Diffusivity of oxygen vacancies

Before calculating the diffusivities of oxygen vacancies in the passive film formed in three solutions, the EIS spectra were measured in different formation potentials (E_f), as shown in Fig. 7a–c.

According to Eq. (9) [21], the thickness of passive film (L_{ss}) at a given passive film formation potential can be obtained by the measurement of EIS plots.

$$L_{ss} = \frac{\varepsilon\varepsilon_0 A}{C_f} \tag{9}$$

where C_f is the passive film capacitance; ε is the relative permittivity of passive film; ε_0 is the permittivity of vacuum; and A is the

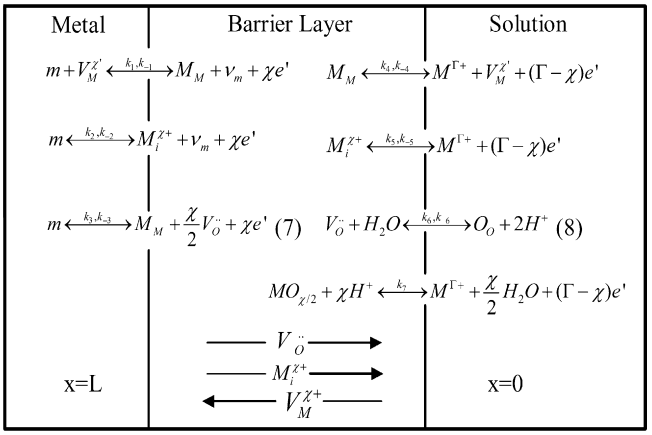

Fig. 6. Interfacial defect generation–annihilation reactions. m, metal atom; V_M'', cation vacancy on the metal sublattice of the barrier layer; $M_i^{\chi+}$, interstitial cation; M_M, metal cation on the metal sublattice of the barrier layer; V_O, oxygen vacancy on the oxygen sublattice of the barrier layer; O_O, oxygen anion on the oxygen sublattice of the barrier layer; $M^{\Gamma+}$, metal cation in solution.

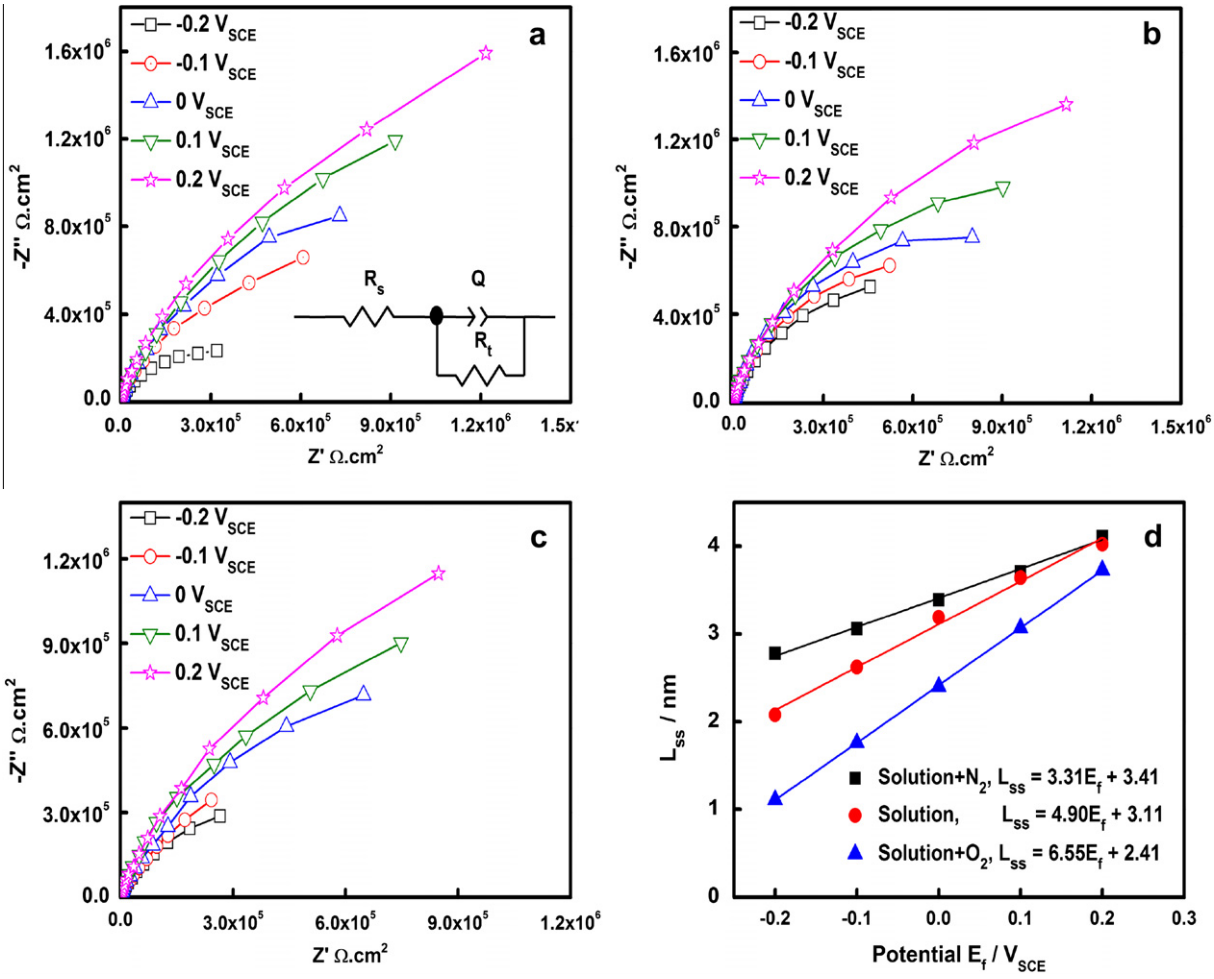

Fig. 7. EIS plots and L_{ss}–E_f curves of 316L SS in solution with different dissolved oxygen. (a) EIS plots in solution with saturated N_2, (b) EIS plots in solution, (c) EIS plots in solution with saturated O_2, (d) the relationship between the thickness of passive film and E_f.

surface area of the sample. Fig. 7d displays the thickness of passive film formed on 316L SS at various E_f. For the three curves, linear relationships between L_{ss} and E_f are indicated, which correspond with Eq. (10) [22]:

$$L_{ss} = \frac{1}{\varepsilon_L}(1-\alpha)E_f + B \tag{10}$$

where α is the polarizability of the passive films/solution interface ($\alpha = 0.743$) [23]; B is a constant; ε_L is the mean electric filed strength, which is a key parameter to calculate the diffusivity of point defects in the film. Three slopes, which represent anodizing constant of the passive film, are 3.31, 4.90 and 6.55 respectively with the increase of dissolved oxygen. It indicates that the thickness of passive film formed on 316L SS in solution with saturated O_2 is most sensitive with increasing of the potential. The ε_L can be calculated from slopes to be 0.78×10^6 V/cm, 0.52×10^6 V/cm and 0.39×10^6 V/cm with the increase of dissolved oxygen.

Based on the PDM, it is been proved that the relationship between the donor density and the film formation potential can be described with [23]:

$$N_d = \omega_1 \exp(-bE_f) + \omega_2 \tag{11}$$

where ω_1, ω_2 and b are unknown constants, which can be determined from the fitting results of N_d–E_f curves. The exponential fitting curves to the experimental data are shown in Fig. 5. The exponential relationship between the N_d and E_f in solution with different dissolved oxygen is listed as:

$$\text{In solution}: \quad N_d = 1.69\exp(-4.94E_f) + 0.90;$$

$$\text{In solution} + N_2: \quad N_d = 1.04\exp(-6.21E_f) + 1.09;$$

$$\text{In solution} + O_2: \quad N_d = 3.08\exp(-3.94E_f) + 0.38.$$

Macdonald also demonstrated that ω_2 in Eq. (11) could be related to the diffusivity of the point defects (mainly oxygen vacancies) D_0 by the following equation based on the Nernst–Plank transport equation:

$$D_0 = \frac{J_0}{2K\omega_2} \tag{12}$$

where J_0 is the steady-state flux of donors, and $K = F\varepsilon_L/(RT)$; F is the Faraday constant; R is the gas constant and T is the temperature. The relationship between J_0 and passive current in steady-state could be expressed with [23]:

$$J_0 = -\frac{i_{ss}}{2e} \tag{13}$$

where i_{ss} is the steady-state passive current density.

Form the Eqs. (9)–(11) and (13), it is easy to calculate diffusivities of oxygen vacancies in the passive film of 316L SS in three solutions, as shown in Table 2. Considering the errors caused by

Table 2
The diffusivities of point defects of passive films formed on 316L SS at each potential in solution with different dissolved oxygen.

Formation potential E_f/V_{SCE}	Solution + N_2		Solution		Solution + O_2	
	i_{ss}/ μA	$10^{-16}D_0$/ $cm^2\ s^{-1}$	i_{ss}/ μA	$10^{-16}D_0$/ $cm^2\ s^{-1}$	i_{ss}/ μA	$10^{-16}D_0$/ $cm^2\ s^{-1}$
−0.2	1.95	0.77	1.15	0.81	7.94	17.70
−0.1	2.96	1.12	1.85	1.30	7.00	15.60
0	3.56	1.40	2.77	1.95	6.47	14.42
0.1	3.72	1.46	3.24	2.28	6.17	13.75
0.2	3.85	1.51	3.47	2.44	6.07	13.53

the fitting curves in Figs. 5 and 7d, D_0 values are estimated to be approximately in the range of 10^{-16} cm^2/s and 10^{-15} cm^2/s, which correspond to the diffusivity of donors determined by Macdonald [23] for WO_{3-x} passive film, 5.3×10^{-15} cm^2/s. In Table 2, it is obvious that D_0 values in solution with saturated O_2 is highest at each formation potential, while D_0 obtained in solution with saturated N_2 is lowest. According the Eqs. (7) and (8) in Fig. 6, higher D_0 is beneficial for metal dissolution. Therefore, the calculated D_0 also demonstrates higher dissolved oxygen in solution accelerate the anodic process.

4. Conclusions

The effects of dissolved oxygen on the electrochemical behavior and semiconductor properties of 316L SS were investigated in 0.05 M H_3BO_3 + 0.075 M $Na_2B_4O_7.10H_2O$ solution. Saturated dissolved oxygen in borate buffer solution accelerates both cathodic and anodic process of 316L SS. The donor densities in the passive film are in the range of $1-7 \times 10^{27}$ m^{-3} and increase with the dissolved oxygen, while the flat-band potential shifts to the negative direction as dissolved oxygen increases. The diffusion coefficient D_0 in three solutions at each potential are calculated to be approximately in the range $1-18 \times 10^{-16}$ cm^2/s. These parameters, donor density N_d, flat-band potential E_{fb} and diffusion coefficient D_0, are useful to explain the effects of dissolved oxygen on the anodic dissolution process of 316L SS.

Acknowledgements

The authors acknowledge the support of China National Natural Science Foundation (No. 50871020). Science & Technology Program of Beijing (No. D09030303790901).

References

[1] Y.X. Qiao, Y.G. Zheng, P.C. Okafor, W. Ke, Electrochim. Acta 54 (2009) 2298–2304.
[2] X.F. Zhu, L. Liu, Y. Song, Mater. Lett. 62 (2008) 4038–4040.
[3] A.C. Crossland, H. Habazaki, K. Shimizu, P. Skeldon, Corros. Sci. 41 (1999) 1945–1954.
[4] D.S. Kong, S.H. Chen, C. Wang, W. Yang, Corros. Sci. 45 (2003) 747–758.
[5] E. Sikora, D.D. Macdonald, Electrochim. Acta 48 (2002) 69–77.
[6] F.J. Martin, G.T. Cheek, W.E.O. Grady, P.M. Natishan, Corros. Sci. 47 (2005) 3187–3201.
[7] J. Amri, T. Souier, B. Malki, B. Baroux, Corros. Sci. 50 (2008) 431–438.
[8] A. Fattah-alhosseini, M.A. Golozar, A. Saatchi, Corros. Sci. 52 (2010) 205–209.
[9] C. Marconnet, Y. Wouters, F. Miserque, C. dagbert, Electrochim. Acta 54 (2008) 123–132.
[10] N.E. Hakiki, S. Boudin, B. Rondot, M. Da Cunha Belo, Corros. Sci. 37 (1995) 1809–1822.
[11] S.R. Morrison, Electrochemistry at Semiconductor and Oxidized Metal Electrodes, Plenum Press, New York, 1980, pp. 49–64, 72–78, 126–128, 154–155, 163.
[12] A.M.P. Simoes, M.G.S. Ferrira, B. Rondot, J. Electrochem. Soc. 137 (1990) 82–87.
[13] M. Buchler, P. Schmuki, H. Bohni, J. Electrochem. Soc. 145 (1998) 609–614.
[14] J. Sikora, E. Sikora, D.D. Macdonald, Electrochim. Acta 45 (2000) 1875–1883.
[15] G.Z. Meng, Y.W. Shao, T. Zhang, Y. Zhang, Electrochim. Acta 53 (2008) 5923–5926.
[16] Valeria A. Alves, Christopher M.A. Brett, Electrochim. Acta 47 (2002) 2081–2091.
[17] J.Q. Kang, Y.F. Yang, X. Jiang, H.X. Shao, Corros. Sci. 50 (2008) 3576–3580.
[18] D.D. Macdonald, J. Electrochem. Soc. 153 (2006) B213–B224.
[19] D.D. Macdonald, J. Nucl. Mater. 379 (2008) 54–58.
[20] M.J. Kloppers, F. Bellucci, R.M. Latanision, Corrosion 48 (1992) 229–238.
[21] E. Sikora, J. Sikora, D.D. Macdonald, Electrochim. Acta 41 (1996) 783–789.
[22] G. Vázquez, I. González, Electrochim. Acta 52 (2007) 6771–6777.
[23] D.D. Macdonald, M. Urquidi-Machonaid, J. Electrochem. Soc. 137 (1990) 2395–2403.